

DETERMINING THE CO-ROTATION RADII OF SPIRAL GALAXIES USING SPIRAL ARM PITCH ANGLE MEASUREMENTS AT MULTIPLE WAVELENGTHS

SHAMEER ABDEEN^{1,2}, DANIEL KENNEFICK^{1,2}, JULIA KENNEFICK^{1,2}, RYAN MILLER³, DOUGLAS W. SHIELDS^{1,2}, ERIK B. MONSON^{1,2} AND BENJAMIN L. DAVIS⁴

First Draft, Jan 30, 2020

ABSTRACT

The spiral arms spanning disk galaxies are believed to be created by density waves that propagate through galactic disks. We present a novel method of finding the co-rotation radius where the spiral arm pattern speed matches the velocities of the stars within the disk. Our method uses an image-overlay technique, which involves tracing the arms of spiral galaxies on images observed in different wavelengths. Density wave theory predicts that spiral arms observed from different wavelengths show a phase crossing at the co-rotation radius. For the purpose of this study, 20 nearby galaxies were analyzed in four different wavelengths with pitch angle measurements performed by two independent methods. We used optical wavelength images (*B*-band 440nm), two infrared wavelength images provided by Spitzer (3.6 μ m and 8 μ m) and ultraviolet images from GALEX (1350 \AA , 1750 \AA). The results were compared and verified with other records found in the literature. We then found rotation curve data for six of our galaxies and used our co-rotation radii estimates to measure the time that would elapse between star formation and moving to their observed positions in the *B*-band spirals. The average time lapse for this motion was found to be ~ 50 Myr. The success of this new method of finding the co-rotation radius confirms density wave theory in a very direct way.

Keywords: galaxies: corotation — galaxies: spiral galaxies— galaxies: density waves

1. INTRODUCTION

The density wave theory, introduced by C.C. Lin & Frank Shu (Lin & Shu 1964; Bertin & Lin 1996; Shu 2016) proposed a theoretical explanation for the existence of spiral structures in galaxies due to long lived quasi-stationary density waves. Subsequent development of the theory has focused on the highly dissipative nature of the galactic disk, which casts doubt on the semi-permanence of the spiral patterns envisaged by the original theory (Toomre 1969). Numerical simulations of density waves in disks have especially fostered the view that spiral patterns created by density waves may be transient in nature (Sellwood & Carlberg 1984), possibly lasting only as long as one or two rotations of the galactic disk (recall that the Milky Way has a rotation period of 250 Myr). Nevertheless some simulations continue to suggest that spiral patterns could be quite long-lived, lasting many rotational periods (Sellwood 2012; Sellwood & Carlberg 2014).

It is not only theorists who disagree on this topic. Observational studies have also contradicted each other upon this point. Foyle et al. (2011) point out that the absence of color gradients in the spiral arms of galaxies would suggest that the density waves are too transient to permit time for such gradients to develop. But the work of Martínez-García & González-Lópezlira (2015) does find evidence for such color gradients and they ar-

gue that the spiral arms must be long-lived. Evidence for these color gradients is presented in Pour-Imani et al. (2016); Miller et al. (2019) using a different approach, which demonstrates that the spiral arm pitch angle in wavebands associated with star-formation is consistently larger than those associated with the stellar population. This suggests that new-born stars are found downstream of the star-formation region in a manner consistent with the density-wave theory. A study by Yu & Ho (2018) with a large number of galaxies strongly confirms this picture and agrees with the work of Martínez-García & González-Lópezlira (2015). Pour-Imani et al. (2016) also agrees with theirs in broad outline (but see Section 4.2 below for one significant detail where they differ).

In this paper, we seek to take advantage of this discovery to further explore the nature of the spiral structure. We show how overlaying the different spiral arms, from the star-forming region and from the stellar arm enables us to find the co-rotation radius (R_{CR}) of a galaxy. Then, for those galaxies for which rotation curves are available, we calculate the time that elapses between stars being born in the star-forming region and then being observed downstream in the *B*-band. This time is found to be a significant fraction of the rotational period of a galaxy, thus suggesting, in agreement with Martínez-García & González-Lópezlira (2015), that the spiral arms cannot be extremely transient.

Due to the differential rotation of the disk, stellar populations move faster than the spiral arm density wave inside the co-rotation radius, while they lag behind the spiral arm density wave outside the co-rotation radius. The general motion of stellar populations about the galactic center can be considered as a motion along an axially symmetric gravitational field, and with a proper selection of an appropriate reference frame, one can express

¹ Department of Physics, University of Arkansas, 226 Physics Building, 825 West Dickson Street, Fayetteville, AR 72701, USA

² Arkansas Center for Space and Planetary Sciences, University of Arkansas, 346 1/2 North Arkansas Avenue, Fayetteville, AR 72701, USA; msabdeen@uark.edu

³ Department of Physics, Utica College, 1600 Burrstone Rd, Utica, NY 13502, USA;

⁴ Centre for Astrophysics and Supercomputing, Swinburne University of Technology, Hawthorn, VIC 3122, Australia

this as an epicyclic motion. The inner Lindblad (ILR) and the outer Lindblad (OLR) resonances are defined in terms of this epicyclic frequency. The pattern speed (Ω_p) and the angular velocity of the disk $\Omega(R)$ are related to the epicyclic frequency κ by the equation, $\Omega_p = \Omega(R) \pm \kappa/2$, where the plus and minus signs give the ILR and the OLR, respectively.

Identifying the location of the co-rotation radius is of central importance to understanding the evolution of the spiral structure. The existence of a co-rotation radius itself serves as evidence of the validity of the density wave theory. Furthermore, since the co-rotation radius acts as a region of resonance or a stable region within the galaxy structure, it has a dynamical influence on the matter and the chemical composition distribution process of the galaxy (Scarano & Lépine 2013). The region of stability around the co-rotation radius creates an ideal environment for a Galactic habitable zone (GHZ) e.g. Marochnik (1983); Sundin (2006). There are multiple papers (Creze & Mennessier 1973; Mishurov & Zenina 1999) among others, that claim to find the location of the Sun close to the galactic co-rotation radius of the Milky Way.

There are many methods of identifying the co-rotation radius. The Tremaine-Weinberg method (Tremaine & Weinberg 1984) hereafter TW, requires certain specific morphological features along with the assumptions (a) the disc of the galaxy is flat, (b) the disc has a well-defined pattern speed, and (c) the surface brightness of the tracer obeys the continuity equation. The TW method directly measures the bar pattern speeds. Using the TW method some authors (Merrifield et al. 2006; Grand et al. 2012) have claimed to observe multiple spiral arm pattern speeds that vary with the radius from the galactic center, which may result in observing multiple co-rotation radii.

Finding the co-rotation radius from morphological features is also a common technique. Elmegreen & Elmegreen (1990) claimed to observe sharp end points to star formation ridges and dust lanes near the co-rotation radius in gas-rich galaxies. Patsis et al. (2003) claimed that rings in spiral galaxies can be related to resonance locations.

Scarano & Lépine (2013) analyzed the relationship between the galactic radius where the metallicity distributions break and the co-rotation radius. Type II supernovae explosions associated with spiral arm density wave propagation are directly responsible for oxygen production. By analyzing oxygen abundance from line fluxes, they were able to find a convincing relationship between the co-rotation radius and the metallicity distribution break radius.

The Puerari & Dottori method (Puerari & Dottori 1997) hereafter PD, uses a photometric method to find the phase crossings in Fourier transforms of azimuthal profiles in B and I bands. The motion of the spiral arm density wave through the galactic disk generates a shock induced star formation process that produces an azimuthal age gradient of stars throughout the spiral arm. Martínez-García et al. (2009) claimed to observe this age gradient in the form of a color gradient flowing azimuthally outwards across the spiral arm flowing in opposite directions on either side of the R_{CR} . Throughout history B , I , HI , CO and FUV wave bands have been used in order to observe this phase shift.

In agreement with the PD method, we were able to introduce a novel way of determining the co-rotation radius, based on an image overlaying technique, which involves tracing the arms of spiral galaxies on images observed from different wavelengths. In a previous study (Pour-Imani et al. 2016), convincing evidence was given in favor of an implication of density wave theory, which states that the pitch angle varies with wavelength for a given galaxy. Thus we have different apparent spiral arms at different wavelengths. Since these spiral arms have different pitch angles, it is possible for them to cross over each other when they are overlaid on the same image of the galactic disk. The crossing-point should be the co-rotation radius. Below we measure the co-rotation radius by this method and compare it to other methods which have been used for our sample and find it is successful at correctly measuring the position of this radius.

2. THE DATA SAMPLE

The accuracy of our method relies on three cardinal criteria. (a) The inclination of the galaxy. If the galaxy has a very high inclination angle, most of the crucial details will be lost in the de-projection process. We selected our galaxies such that the inclination angles are $\leq 60^\circ$. (b) Well defined spiral structure. The overlaying technique requires the galaxy sample to have a well-defined, clear spiral structure in order to accurately overlay the synthetic spirals. (c) The variation of the spiral arm pitch angle with the galactic radius remains constant for a significant proportion of the galactic radius. This amounts to a criterion that the spiral arms are logarithmic spirals. Although we assign a mean value for the pitch angle, the extent to which the spiral arms are intrinsically logarithmic plays a vital role in this criterion.

Our galaxy sample (see Table 1) was selected based on the availability of co-rotation radii measurements in the literature, along with considering the above mentioned criteria. Twenty nearby galaxies were analyzed in four different wave bands. Twelve galaxies were selected from the galaxy sample of Scarano & Lépine (Scarano & Lépine 2013) while the remaining eight galaxies were selected from Buta & Zhang (2009). We used optical wavelength images (B -band 440nm), two infrared wavelengths ($3.6\mu\text{m}$ and $8\mu\text{m}$) from the Spitzer Infrared Nearby Galaxies Survey (SINGS)¹, and ultraviolet images from Galaxy Evolution Explorer (GALEX)². For 12 galaxies, the distances were recorded based on the compilations of Scarano & Lépine (Scarano & Lépine 2013). Our galaxy sample was limited to a distance of 36.8 Mpc ($z = 0.007942$), where NGC 7479 had the furthest recorded distance.

3. ANALYSIS

3.1. De-projecting and Measuring Pitch Angles

Galaxies with non-zero inclination angles between the plane of sight and their disks had to be de-projected to a face-on orientation. Since we were working with four different wavelengths, we first created a composite image. Using the composite image we used the traditional approach of fitting elliptical isophotes and then transformed them to a circular configuration. We used the

¹ <https://irsa.ipac.caltech.edu/data/SPITZER/SINGS/>

² <https://archive.stsci.edu/missions-and-data/galex-1/>

Table 1
Sample

Galaxy Name (1)	Hubble Type (2)	RA (J2000) (3)	Dec(J2000) (4)	Distance (Mpc) (5)	Method (6)	Image Sources (7)
NGC 0628	SA(s)c	01 36 41.7	+15 47 01	6.7	SNII*	[1],[2],[3],[5]
NGC 2403	SAB(s)cd	07 36 51.4	+65 36 09	3.47	SNII*	[1],[2],[3],[6]
NGC 3031	SA(s)ab	09 55 33.2	+69 03 55	3.63	Cph*	[1],[2],[3],[7]
NGC 2903	SAB(rs)bc	09 32 10.1	+21 30 03	6.52	Hub*	[1],[2],[3],[8]
NGC 4254	SA(s)c	12 18 49.6	+14 24 59	32.30	Hub*	[1],[2],[4],[9]
NGC 5194	SA(s)bc	13 29 52.7	+47 11 43	8.9	SNII*	[1],[2],[3],[8]
NGC 5236	SAB(s)c	13 37 00.9	-29 51 56	4.5	Cph*	[1],[2],[3],[10]
NGC 5457	SAB(rs)cd	14 03 12.5	+54 20 56	7.4	Cph*	[1],[2],[3],[8]
NGC 1566	SAB(s)bc	04 20 00.4	-54 56 16	18.2	Hub*	[1],[2],[3],[11]
NGC 4321	SAB(s)bc	12 22 54.8	+15 49 19	16.10	Cph*	[1],[2],[3],[7]
NGC 5033	SA(s)c	13 13 27.4	+36 35 38	12.7	Hub*	[1],[2],[8]
NGC 6946	SAB(rs)cd	20 34 52.3	+60 09 14	3.76	Hub*	[1],[2],[12]
NGC 1042	SAB(rs)cd	02 40 24.0	-08 26 01	15.0	Tully-Fisher	[1],[3],[12]
NGC 4579	SAB(rs)b	12 37 43.5	+11 49 05	16.7	Tully-Fisher	[1],[3],[12]
NGC 5701	(R)SB(rs)0/a	14 39 11.1	+05 21 49	15.4	Tully-Fisher	[1],[3],[13]
NGC 5850	SB(r)b	15 07 07.7	+01 32 39	18.7	Tully-Fisher	[1],[2],[12]
NGC 3938	SA(s)c	11 52 49.4	+44 07 15	21.9	SNII	[1],[2],[8]
NGC 4136	SAB(r)c	12 09 17.7	+29 55 39	9.7	Tully-Fisher	[1],[3],[12]
NGC 7479	SB(s)c	23 04 56.6	+12 19 22	36.8	Tully-Fisher	[1],[3],[12]
NGC 7552	(R')SB(s)ab	23 16 10.7	-42 35 05	14.8	Tully-Fisher	[1],[2],[10]

Note. — Columns: (1) Galaxy name (2) Hubble morphological type (3) RA (J2000) (4) DEC (J2000) (5) Distance (Mpc) (6) Method for distance calculations (* Distance and Method for distance calculations are based on the compilations of Scarano & Lépine (Scarano & Lépine 2013)) (7) Image Sources (Telescope/wavelength): [1]=IRAC 3.6 μ m,[2]=IRAC 8.0 μ m,[3]=GALEX 1516Å,[4]=GALEX 1542Å, [5]=NOT 4400Å,[6]=LCO 4400Å,[7]=WIYN 4331Å,[8]=KPNO 4400Å,[9]=INT 4034Å, [10]=CTIO 4400Å,[11]= duPont 4400Å,[12]=JKT 4034Å,[13] = Lowell1.1m 4500Å

de-projecting parameters of the composite image, namely the position angle and the ellipticity and applied them to each individual wavelength image.

The pitch angle of a spiral is defined as the angle between the spiral's tangent at a given point and the tangent line drawn to a concentric circle with the center located at the galactic center, that passes through that point. Pitch angle measurements were performed by two independent methods namely 2DFFT method (Seigar et al. 2008; Davis et al. 2012) and the SPIRALITY (Shields et al. 2015)³ method. The 2DFFT method uses a modified two dimensional fast Fourier transform process to generate the pitch angles as a function of galaxy radius in pixels for different harmonic modes. Figure 1 shows the variation of pitch angle with radius (galactocentric offsets) in NGC 5194 for the second harmonic mode. NGC 5194 is an example of a galaxy that has a small relative difference in the variation of the pitch angles in all four wavelengths, hence giving rise to nearly equal mean pitch angles (see NGC 5194 in Table2) while NGC 628 is an example of a galaxy that has a larger relative difference in mean pitch angles (see Figure 2 and Table 2). Visually confirming the accuracy of our pitch angle measurements, can be done by performing an inverse fast Fourier transformation (Davis et al. 2012) (Figure 3). SPIRALITY is a MATLAB code designed to measure pitch angles using a template fitting approach. Within the measurement annulus, SPIRALITY uses a variable inner radius method and focuses on a global best-fit pitch. For six galaxies, pitch angles were adopted from a previous study by Pour-Imani et al. (2016), which had also used the same techniques to measure the pitch angles.

The results were visually verified again by using a Python script (SPIRAL_OVERLAY.PY, hereafter OL SCRIPT)⁴.

3.2. Astrometric Accuracy

Astrometric precision plays a vital role when overlapping images of different wavelengths and analyzing their characteristics. Figure 4 represents the offset distributions of point sources in NGC 5194, each wavelength compared against, *B*-band. As the initial process, point sources were identified in each image using the DAOSStarFinder class of the photutils package in ASTROPY. DAOSStarFinder uses the DAOFIND (Stetson 1987) algorithm which searches images for local intensity maxima with peak amplitudes greater than a given threshold value. After identifying the point sources, we searched for common points which were detected in both wavelengths. Once we have a list of common point sources, we can find the relative offsets in ΔRA and ΔDEC . Considering the total data set, the mean of ΔRA is -0.2109 arcsec and the mean of ΔDEC is 0.0015 arcsec.

3.3. Tracing the Individual Images

The overlaying technique consists of two main steps. The first step involves tracing the spiral arms on all four images (corresponding to the four wavebands). This process was done by two independent methods. One using the above mentioned OL SCRIPT and the other utilizing, SPIRALITY; SPIRAL ARM COUNT (Shields et al. 2015) script. In order to incorporate the uncertainties of the pitch angles each image was traced twice, using the

³ Spirality: <http://ascl.net/phpBB3/download/file.php?id=29>

⁴ Python OL Script: <https://github.com/ebmonson/2DFFTUtils-Module>

Table 2
Average Pitch Angle Measurements

Galaxy Name (1)	i° (2)	PA° (3)	P° (IRAC 3.6) (4)	P° (B-band) (5)	P° (IRAC 8.0) (6)	P° (FUV-band) (7)
NGC 0628	7	20	13.56 ± 2.21	13.94 ± 0.64	12.83 ± 0.66	12.81 ± 0.65
NGC 3031	44	150	12.75 ± 2.31	13.32 ± 2.17	12.58 ± 1.22	16.20 ± 5.63
NGC 2903	38.24	22.12	23.62 ± 1.32	23.97 ± 1.03	24.23 ± 1.16	24.49 ± 2.25
NGC 4254	23.76	58.83	21.04 ± 1.67	22.45 ± 1.68	20.50 ± 1.73	20.39 ± 3.59
NGC 5194	21.96	28.02	9.66 ± 2.17	10.21 ± 2.7	10.48 ± 2.73	12.89 ± 2.53
NGC 5236	5.11	-49.96	10.56 ± 1.78	10.63 ± 1.27	11.71 ± 1.95	12.92 ± 1.10
NGC 5457	7.64	4.01	22.77 ± 1.24	23.33 ± 1.28	23.85 ± 1.65	24.13 ± 2.94
NGC 1566	12.12	178	19.95 ± 1.84	18.23 ± 1.74	22.37 ± 1.54	18.90 ± 1.99
NGC 4321	25.9	-53.14	16.07 ± 2.42	16.05 ± 2.75	14.73 ± 1.68	14.40 ± 1.58
NGC 5033	43.71	4.26	7.09 ± 0.46	10.46 ± 2.66	13.91 ± 4.42	-
NGC 6946	9.2	-88.82	22.02 ± 1.02	24.10 ± 1.8	24.63 ± 2.01	-
NGC 1042	43	118	20.05 ± 2.16	22.39 ± 1.33	-	25.71 ± 1.29
NGC 4579	46	75	20.35 ± 1.24	18.18 ± 1.16	-	24.8 ± 1.27
NGC 5701	54	174	9.38 ± 1.03	8.08 ± 1.57	-	10.52 ± 1.35
NGC 5850	24	-44	8.46 ± 0.14	7.39 ± 1.47	13.22 ± 0.30	-
NGC 3938	15	27	13.02 ± 0.70	13.52 ± 1.38	16.67 ± 1.98	-
NGC 4136	2	-79	10.07 ± 1.06	12.06 ± 2.16	-	15.68 ± 3.16
NGC 7479	18	37	14.14 ± 1.21	15.74 ± 1.49	-	16.47 ± 3.37
NGC 7552	19	-76.98	25.87 ± 3.67	27.58 ± 3.38	28.99 ± 2.83	-

Note. — Columns: (1) Galaxy name; (2) inclination angle in degrees (3) Position angle in degrees (4) pitch angle in degrees for Spitzer 3.6 μm ; (5) pitch angle in degrees for B-band; (6) pitch angle in degrees for Spitzer 8.0 μm ; (7) pitch angle in degrees for FUV-band;

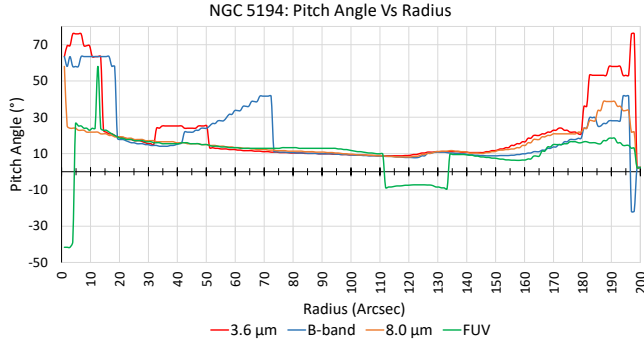


Figure 1. The graph of the pitch angle variation, as a function of radius for NGC 5194.

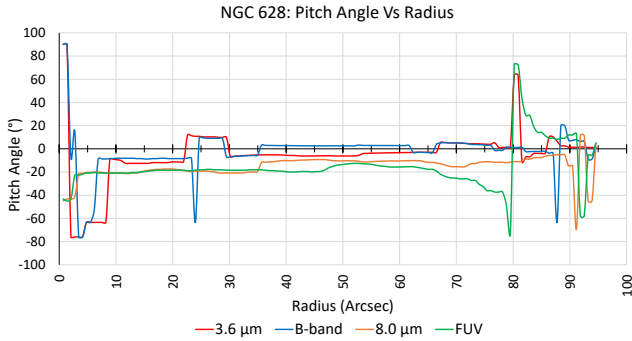


Figure 2. The graph of the pitch angle variation, as a function of galaxy radius for NGC 628. The graphs in figure 1 and 2 were created using the results from the 2DFFT method.

maximum and the minimum pitch angle uncertainties, giving rise to two image arrays. Since the tracing was done by using the maximum and the minimum image arrays, the uncertainties of the pitch angles play a vital role in this phase.

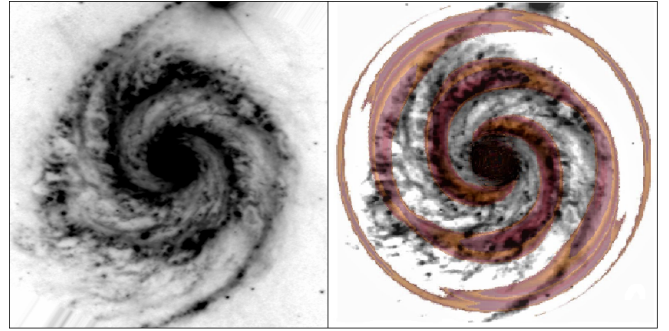


Figure 3. NGC 5194 along with its inverse 2DFFT output overlaid on the original image.

3.3.1. Using the PYTHON OL SCRIPT

The PYTHON OL SCRIPT generates a graphical interface that enables us to load a FITS image, along with a synthetic logarithmic spiral placed on a foreground layer. Pitch angle, phase angle, the chirality (the direction in which galaxies appear to be) and the number of arms are among the parameters that are available for variation. Since the chirality, the number of arms, and pitch angles are known (through visual observations and using Table 2), the logarithmic spirals with the appropriate pitch angles can be precisely traced over the actual image by changing only the phase angle (see Figure 5). The accuracy of this process depends on the image clarity of the spiral arms and the contrast they show between the arm and inter-arm regions. As discussed, the extent to which the spiral arms are intrinsically logarithmic also plays an important role in the tracing process. Since the overlaying synthetic spiral traces are logarithmic, if the actual spiral structure of the galaxy has intrinsic deviations from being logarithmic, the overlaying would not be accurate.

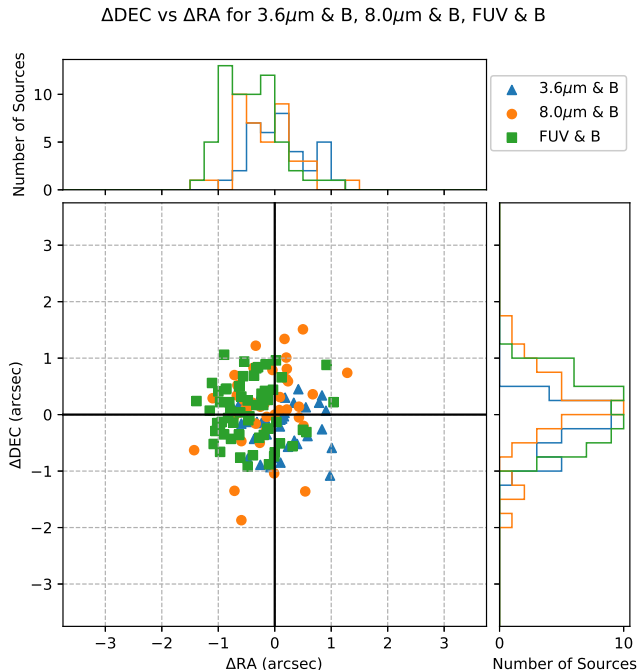


Figure 4. Measured relative offsets of point sources in NGC 5194, for wavelengths $3.6\mu\text{m}$, $8.0\mu\text{m}$ and FUV , compared against B -band. Considering the total data set, the mean of ΔRA is -0.2109 arcsec and the mean of ΔDEC is 0.0015 arcsec.

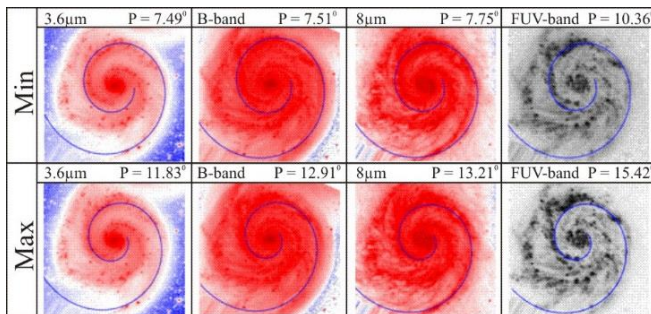


Figure 5. Incorporating the uncertainties of the pitch angles, each image was traced twice, adding the positive and the negative uncertainties, giving rise to two image arrays corresponding to the maximum and minimum pitch angles. The PYTHON OL SCRIPT was used to create these images.

3.3.2. Using the SPIRALITY; SPIRAL ARM-COUNT-SCRIPT

SPIRALITY, SPIRAL-ARM-COUNT (Shields et al. 2015) script is a MATLAB script that fits logarithmic spiral arms traced over images based on image pixel brightness. As the name suggests the SPIRAL-ARM-COUNT script has the capability of measuring the number of arms in a given spiral galaxy image. It also produces a graph of phase angle vs median relative pixel values where the maxima turning points corresponds to the brightest regions of the spiral arms (see Figure 6).

3.3.3. Trace Accuracy

In order to quantify the accuracy of the tracing process, we defined the measurement “Trace accuracy”, the ratio of the stable pitch angle region compared with the length of the spiral arm, expressed as a percentage.

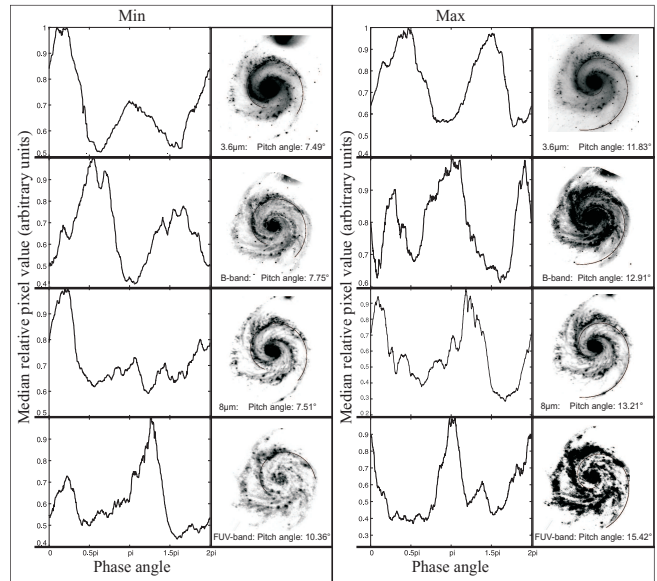


Figure 6. Max and min image arrays produced using the SPIRALITY, SPIRAL-ARM-COUNT script. A graph of phase angle vs median relative pixel values is depicted, corresponding to each image. The locations of the maxima turning points correspond to bright regions of the spiral arms.

$$\text{Trace accuracy} = \frac{(\text{Stable pitch angle region})}{(\text{Length of the spiral arm})} \times 100\%$$

Higher trace accuracy simply implies a more reliable trace. Since the overlaying synthetic spiral traces are logarithmic, the extent to which the underlying galactic spiral arms are intrinsically logarithmic plays a vital role in having a higher trace accuracy. It is also important to note that well-defined spiral structures tend to have higher trace accuracies in comparison to flocculent galaxies. In our sample of 20 galaxies, four galaxies showed trace accuracies less than 40%, while NGC 2403 and NGC 1566 showed the lowest trace accuracies for all the bands.

3.4. Overlaying

Once we have all the individual images traced, the next step is overlaying the images and identifying the locations where the traced arms intercept each other. This process was done yet again by two independent methods. The first method involved the PYTHON OL SCRIPT, in which all the images were loaded as layers, saving one image at a time as a image. The second method used the RGB image creating capability of DS9 to construct the composite images. Individually traced images of different wavelengths were loaded as red, green and blue images in constructing the composite RGB image, giving preference to the images that gave the maximum outer extent of the R_{CR} and the minimum inner extent of the R_{CR} .

4. RESULTS

The median radii (depicted by the red circle in the rightmost panels of Figure 7) were calculated by considering the maximum outer extent of the R_{CR} and the minimum inner extent of the R_{CR} (depicted by the two blue circles in the rightmost panels of Figure 7). The

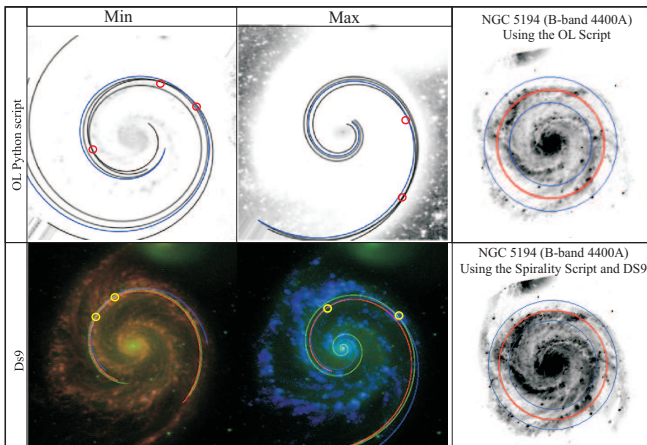


Figure 7. The individually traced images are overlaid in the form of an RGB image using DS9. The locations in which the traced spiral arms intercept, correspond to the inner and the outer parts of the co-rotation radius.

R_{CR} results that we obtained using the two independent methods were compared against the mean values compiled from the literature (see Figure 8). The mean values obtained from the literature are as summarized by Scarano & Lépine (2013) and Buta & Zhang (2009). We can consider the mean and the standard deviations of the normalized R_{CR} values as a measurement of the overall accuracy of our results. Defining normalized R_{CR} as

$$NR_{cr}(OL : Lit) = \frac{R_{cr}(Overlay)}{R_{cr}(Literature)}$$

$$NR_{cr}(SP : Lit) = \frac{R_{cr}(Spirality)}{R_{cr}(Literature)}$$

For OL SCRIPT and SPIRALITY, we found the mean normalized R_{CR} values to be 0.997 and 0.966 respectively. The standard deviations were found to be 0.357 and 0.267 respectively. Although few galaxies (e.g. NGC 5457, NGC 3031) showed significant deviations from the expected values, most of our results were in agreement with the compiled results. The final results are summarized in Table 3. The very fact that we were able to infer the R_{CR} locations from this method serves as a compelling evidence in favor of the implications of density wave theory.

4.1. Time Lapse Calculations

Once we had the co-rotation radius and the individual images with the spiral arms traced, we used them to estimate the overall time lapse between the motion of young arbitrary stars, born at the density wave, to move to their current locations. The time-lapse estimations were done using the $8.0\mu\text{m}$ and B -band traced images of six galaxies in our sample and using published rotation curves in the literature (Daigle et al. 2006). Since the $8.0\mu\text{m}$ wavelength images trace emission from the dust and gas dominated regions, we may use it to portray the current location of the density wave. The B -band images can be used to locate the newly formed stars that are not obscured by dust. Assuming the azimuthal motion of the stars along the disk is circular in nature and assuming a

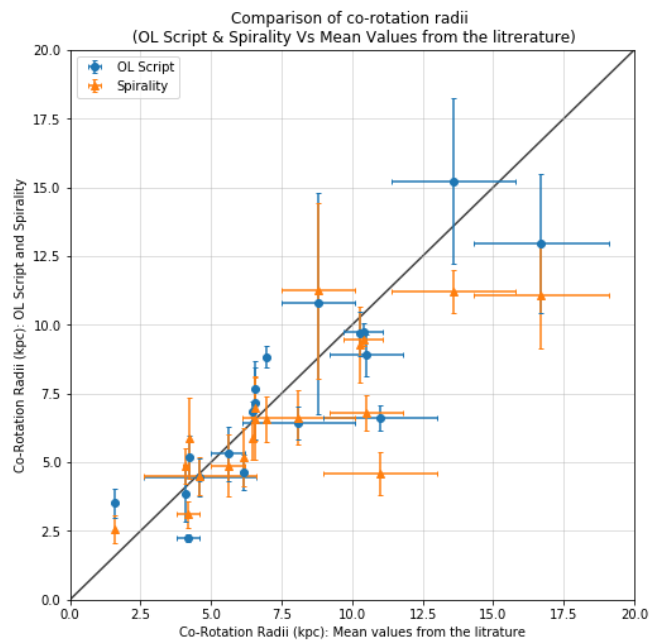


Figure 8. A comparison of co-rotation radii, the blue data points indicates the results from the Overlaying OL SCRIPT method while the red data points indicates the results obtained from the SPIRALITY: SPIRAL ARM COUNT method. The two results are compared against the mean values obtained from the literature (as summarized by Buta & Zhang (2009) and Scarano & Lépine (2013)).

constant pattern speed for the density wave, we analyzed the motion by selecting different radii, both from inside and outside the co-rotation radius (for a particular example consider NGC 5194, see Figure 9 (left)). The angular velocity at the co-rotation radius was used as the global pattern speed of the density wave. The rotation curves were used to identify the angular velocities (see Figure 9 (right)) and hence the relative velocities, between the orbiting particles and the density wave, corresponding to each radii. Using the relative velocities, we were able to estimate the overall mean time lapse for this motion (see Table 4). It is important to note that we should exclude the region close to the co-rotation radius in this process. The overall mean time lapsed range from a minimum of 33.61 Myr to a maximum of 57.80 Myr. The average time lapse for this motion was 48.7 Myr. Depending on the mass of a star, an average B-type star may have a life span of 10-100 million years, hence our calculations are consistent with the current established predictions.

It is important to mention that although we assumed the spiral structures to have a constant pattern speed, we did not discuss the validity of this assumption. Peterken et al. (2019), shows convincing evidence for a constant global pattern speed using $H\alpha$ regions to depict the on-going star formations and considering the offsets with the young stars (less than 60Myr, traced by 4020\AA). They found that the pattern speed (Ω_P) varies very little, with the radius and they further claim that the existence of the constant global pattern speed can be used as evidence in favor of the quasi-stationary density wave theory.

4.2. Comparison with Results from Other Research

As we have seen, using spiral arm pitch angle measurements at different wavelengths as a method to find the co-rotation radius agrees quite well with established

Table 3
A comparison of our results against mean values obtained from literature

Galaxy Name	Rcr: OL Script (kpc)	Rcr: SP Script (kpc)	Rcr: Mean from Lit. (kpc)	$NR_{cr}(OL : Lit)$	$NR_{cr}(SP : Lit)$
NGC 0628	4.45 ± 0.68	4.50 ± 0.68	4.6 ± 2	0.97	0.76
NGC 3031	6.61 ± 0.46	4.59 ± 0.80	11 ± 2	0.60	0.54
NGC 2903	3.87 ± 1.02	4.86 ± 0.64	4.1 ± 0.1	0.94	1.19
NGC 4254	15.23 ± 3.00	11.22 ± 0.78	13.6 ± 2.2	1.12	1.17
NGC 5194	5.31 ± 0.98	4.88 ± 1.12	5.6 ± 0.6	0.95	0.87
NGC 5236	6.44 ± 0.61	6.63 ± 1.00	8.1 ± 2	0.79	0.82
NGC 5457	12.94 ± 2.53	11.06 ± 1.9	16.7 ± 2.4	0.77	0.66
NGC 1566	10.78 ± 4.01	11.24 ± 3.21	8.8 ± 1.3	1.22	1.28
NGC 4321	8.90 ± 0.75	6.81 ± 0.64	10.5 ± 1.3	0.85	1.14
NGC 5033	9.75 ± 0.33	9.48 ± 0.24	10.4 ± 0.7	0.94	0.91
NGC 6946	2.26 ± 0.14	3.11 ± 0.48	4.2 ± 0.4	0.54	0.74
NGC 1042	4.64 ± 0.63	5.20 ± 1.06	6.14*	0.76	0.85
NGC 4579	7.15 ± 1.31	6.58 ± 1.49	6.58*	1.09	1.00
NGC 5701	6.86 ± 0.35	5.88 ± 0.77	6.48*	1.06	0.91
NGC 5850	8.84 ± 0.38	6.57 ± 0.84	6.96*	1.27	0.94
NGC 3938	7.68 ± 1.00	6.97 ± 1.17	6.55*	1.17	1.06
NGC 4136	3.51 ± 0.51	2.55 ± 0.50	1.60*	2.19	1.59
NGC 7479	9.68 ± 0.80	9.27 ± 1.37	10.29*	0.94	0.90
NGC 7552	5.17 ± 0.78	5.86 ± 1.47	4.23*	1.22	1.39

Note. — Columns: (1) Galaxy name; (2) Results from the Overlaying OL SCRIPT method; (3) Results from the SPIRALITY: SPIRAL ARM COUNT method; (4) Mean values obtained from the literature (as summarized by (Scarano & Lépine 2013) and * (Buta & Zhang 2009)); (5) Normalized R_{cr} for OL Script vs Mean from Lit $NR_{cr}(OL : Lit)$; (6) Normalized R_{cr} for SP Script vs Mean from Lit $NR_{cr}(SP : Lit)$.

Table 4
Time lapse calculations

Galaxy Name (1)	Rcr: Spirality Script (kpc) (2)	Ω_p (km/s/kpc) (3)	Mean Relative Velocity (pc/Myrs) (4)	Mean Time Lapse (Myrs) (5)
NGC 0628	4.50 ± 0.68	33.51 ± 10.65	44.24 ± 15.05	33.61 ± 3.84
NGC 3031	4.59 ± 0.80	40.23 ± 4.87	28.24 ± 3.63	48.62 ± 2.73
NGC 5194	4.88 ± 1.12	21.56 ± 6.13	26.84 ± 8.35	54.62 ± 8.75
NGC 4321	6.81 ± 0.64	26.21 ± 4.62	31.42 ± 5.73	43.86 ± 2.69
NGC 6946	3.11 ± 0.48	51.78 ± 10.00	13.63 ± 2.95	57.80 ± 3.79

Note. — Columns: (1) Galaxy name; (2) Rcr: Results from the SPIRALITY: SPIRAL ARM COUNT method; (3) Patern Speed Ω_p ; (4) Mean relative velocity of a young arbitrary star that was born at the density wave (peak intensity isophotes of the $8\mu\text{m}$ image) to the current location (peak intensity isophotes of the B -band image); (5) The overall mean time lapses for the motion of a young arbitrary star that was born at the density wave (peak intensity isophotes of the $8\mu\text{m}$ image) to the current location (peak intensity isophotes of the B -band image).

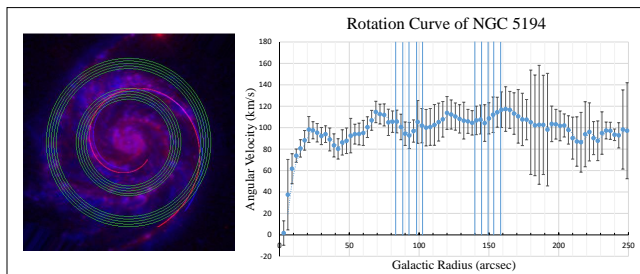


Figure 9. (Left) The locations of the selected radii for the time lapse calculations on the galaxy NGC5194. 10 radii were selected both from inside and outside of the co-rotation radius. (Right) The rotation curve used, Daigle et al. (2006).

techniques. Naturally, this tends to confirm the existence of a color gradient in spiral arms in disk galaxies. It lends confidence in our ability to accurately distinguish between the upstream and the downstream spiral arms. Nevertheless, there are skeptics who doubt the existence of such a gradient. Some researchers argue that there is no consistent color gradient even within local stretches of spiral arms in a given galaxy. By contrast,

several studies, which use pitch angle measurements to try to study the entire length of the spiral arm, agree that there is evidence for a consistent color gradient. Recently a particularly large study by Yu & Ho (2018) added to the growing body of evidence on this point. They find a consistent color gradient and present a model which illustrates how a red and a blue spiral arm (called by them respectively, the potential or P arm and the star-formation or SF arm) will cross each other at the co-rotation radius. In their model the downstream arm contains stars which have moved from the upstream star-forming region over a timescale of 10 Myr or so.

In one respect, Yu & Ho (2018) disagree with the earlier results reported in Pour-Imani et al. (2016)/Miller et al. (2019), find that the infrared pitch angle is generally looser (not tighter, as we find in this paper, in agreement with Miller et al. (2019)) than the pitch angle as measured in other wavelengths, such as B -band. This is consistent with the red spiral arm being generated by old disk stars crowded closer together by the peak of the density wave's spiral potential. Yu & Ho (2018) calls this the color gradient from red to blue and we in con-

trast see what they call an age gradient, of young stars seen downstream from the star-formation region, from blue to red. Yu and Ho contend that the age gradient is not really visible and believe that our measurements of infra-red pitch angles are marred by errors. In one particular case they are undoubtedly right. NGC 1566 is a galaxy found in both their sample and the one in Pour-Imani et al. (2016), for which the pitch angle measurements are in sharp disagreement. Yu & Ho (2018) argue that this is because of a failure to properly choose consistent galaxy parameters, such as galaxy center, ellipticity, position angle, and radius range throughout the different wavelengths that are used, and they are right. We discovered that for six of the galaxies in that sample, the inclinations that we used were not consistent with the ones used by Yu & Ho (2018). For one of these galaxies (NGC 1566) redoing the measurements more carefully with consistent galaxy parameters results in a change of values which agrees better with Yu and Ho’s results, and with their findings on the color gradient. However, we should also point out, as Yu & Ho (2018) did not, that NGC 1566 is not the only galaxy common to the samples of their paper and Pour-Imani et al. (2016). NGC 1097 is also, and in that case our figures agree quite well and the color gradient observed is in agreement with the trend we see (though not strongly).

Another galaxy which is common to Yu & Ho (2018) and our sample is NGC 7552. In this case there is also a considerable disagreement for the $3.6\mu\text{m}$ and B -band measurements, since the values given in Yu & Ho (2018) are $9.7 \pm 1.1^\circ$ and $9.7 \pm 0.9^\circ$ respectively while our values are $25.87 \pm 3.67^\circ$ and $27.58 \pm 3.38^\circ$ (Figure 10). However Yu & Ho (2018) gives only measurements for their 1DFFT method. Apparently their 2DFFT algorithm did not return a value for this galaxy, which might be because it has a long bar. Both of our methods (2DFFT and SPIRALITY) agree in this case. In order to check further we made use of an entirely independent code, SpArcFiRe, which returned a value of $27.03 \pm 3.85^\circ$ for $3.6\mu\text{m}$, compatible with our results, but not with the values given by Yu & Ho (2018). Although it is not always trivial to compare results between these papers, and although there is a consistent disagreement over pitch angle measured in the near infrared ($3.6\mu\text{m}$), the broader picture of distinct upstream and downstream arms emerging from both studies is well confirmed by the work in this paper, in which this result is used successfully to locate the co-rotation radius of a significant sample of disk galaxies. Nevertheless inconsistencies such as the disagreement on the location of the $3.6\mu\text{m}$ infrared arm will provide some comfort for those who favor the transient picture of spiral arms.

Obviously, further work (and more careful work!) is needed to decide this issue. But notice that the disagreement over the pitch angle of the infrared spiral arm is not particularly relevant to the work discussed in this paper. We qualitatively (and wholeheartedly) agree with the model presented, for instance, in Fig. 6 of Yu & Ho (2018), except that we would use star-formation tracers such as FUV or $8\mu\text{m}$ to identify the upstream arm (their P arm) and B -band images to find the downstream arm (their SF arm). The spirit of this paper, therefore, is actually to see if the measured spiral arms actually perform as one would expect given a model similar in spirit

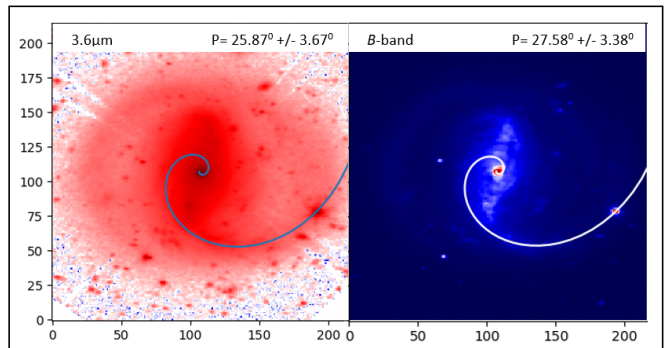


Figure 10. (left) $3.6\mu\text{m}$ image of NGC 7552 along with a synthetic logarithmic spiral of pitch angle $25.87 \pm 3.67^\circ$ traced over the brightest arm. (right) B -band image of NGC 7552 along with a synthetic logarithmic spiral of pitch angle $27.58 \pm 3.38^\circ$ traced over the brightest arm.

to the one discussed in section 4.3 of Yu & Ho (2018). Our answer is an emphatic yes. Invariably tracing of the two spiral arms measured by us does correctly identify the position of the co-rotation radius. We find the elapsed time between the two arm positions to be something in the range of 50 Myr, not too far from the 10 Myr assumed in model presented in Yu & Ho (2018). Therefore, in spite of certain disagreements in detail, we find that the evidence is quite strong for the idea that the color gradient predicted by density wave theory is real. Of course, continued disagreement over the detail leaves an opening for those who argue that there is no consistent age/color gradient. This issue is important because it has been proposed, Yuan & Grosbol (1981) that a consistent age/color gradient supports the theory that spiral arms are long-standing, while no consistent color gradient supports the theory that spiral arms are transient.

Recent work looking for observational evidence on this subject has been divided. Foyle et al. (2011) take the view that there is no evidence for the sort of color-gradient structure that we see and conclude that spiral structure is transient (their work differs from ours in examining local structure within each arm, whereas we look at the full extent of the spiral arm). By contrast, Martínez-García & González-Lópezlira (2015) reach the opposite conclusion, using similar methods. Our work, though very different in approach, seems to be more reconcilable with the Martínez-García and González-Lópezlira conclusion.

5. SUMMARY AND CONCLUSION

We have confirmed the validity of density wave theory in a very direct way by using differently colored spiral arms to find the co-rotation radius and showing that it agrees well with other methods commonly used. This shows the existence of a color gradient demanded by the theory and shows that the spiral arm patterns themselves can be used as a research tool. It therefore is implicit that the arms have a certain reality which is suggested by their success in measurement.

We have compared our results with several methods used to identify the location of the co-rotation radius in a galaxy, with considerable success. It is true that errors in the pitch angle measurements translate to considerable errors in the measurement of the co-rotation radius. We do not propose that our method should supplant other

methods of finding the co-rotation radius. But it is clear that our method is usually accurate and always qualitatively plausible. Even when it is not perfectly accurate, it is not too far off. The argument is that the success in finding the co-rotation radius, that these arms are genuine features created by the underlying density wave.

A major point of debate about the density-wave theory concerns how long the spiral patterns generated by density waves last. The original Lin-Shu theory proposed that the spiral arms were semi-permanent standing-wave patterns, created by resonant modes reflecting back and forth between the inner and outer Lindblad resonances of the disk. Most experts no longer think this is likely. The system seems too dissipative for standing waves to persist indefinitely. Certainly this is what numerical simulations seem to suggest. Indeed it is unclear how such disk-spanning patterns can be excited at all, though the favored mechanisms are external harassment (by another galaxy passing nearby and stimulating a disturbance) or swing amplification (by which small internal perturbations might be amplified) (Toomre 1969). Since it is empirically apparent that the patterns do form, the key question is how long they last.

Some experts, such as Sellwood and Carlberg (Sellwood & Carlberg 2014), argue that the patterns can be quite long-lasting, perhaps for as many as ten galactic rotations. But there is quite a common belief that they may be quite transient, perhaps lasting only one or two rotations of the disk. Our work suggests that it takes on the order of 50 Myr for the spiral pattern defined by the *B*-band to form. When that stellar arm has formed, the original star-forming region can still be seen. This suggests that the spiral arm is a minimum of 50 Myr old. Obviously this is less than a galactic rotation (the Milky Way takes about 250 Myr to rotate once). However, for most of our galaxies we do see a double pattern of this type, which suggests that it is rare to catch a galaxy as the density wave pattern is breaking up. Though we cannot be sure, this does suggest that the typical age of a spiral pattern is several times 50 Myr. This does at least place some lower limit on how transient these patterns can be. It is hard to see how they can generally persist only for one rotation, and even two might be a reasonable lower limit.

Finally, it should be noted that the overall mean time lapses for the motion of a young star from the star-forming region to the *B*-band is consistent with our evolutionary understanding of this process. We would expect the time involved to be longer than 10 million years, so that the shortest-lived O type stars would still be seen in the immediate vicinity of the star-forming region, since they live only a few million years. This is consistent with the fact that our far UV images return pitch angles consistent with the far IR pitch angles (see Miller et al. (2019), for a more detailed discussion). At the same time, we expect that the time elapsed will be less than 100 million years, so that many bright stars will survive to be observable when it is viewed in the *B*-band. All of the values we have obtained for the time elapsed to move between the star-formation arm and

the *B*-band lie between these two values, in the tens of million years, with an average close to 50 Myr (see Table 4). We believe that the overall interpretation we give of our results is consistent with relatively long-lasting density waves.

The authors gratefully acknowledge Bret Lehmer, Rafael Eufrazio, Marc Seigar and Joel Berrier for giving suggestions and contributing to this paper in numerous ways. We would like to thank Iv nio Puerari for writing the original 2DFFT code on which the later versions of 2DFFT was based. We would also like to thank all the members of the Arkansas Galaxy Evolution Survey (AGES) team for their continuous support. This research has made use of the NASA/IPAC Extragalactic Database (NED) and the NASA’s Astrophysics Data System.

REFERENCES

- Bertin, G. & Lin, C. C. 1995, *Spiral structure in galaxies a density wave theory*, The MIT Press
- Buta, R. J., & Zhang, X. 2009, *ApJS*, 182, 559
- Creze, M., & Mennessier, M. O. 1973, *A&A*, 27, 281
- Daigle, O., Carignan, C., Amram, P., et al. 2006, *MNRAS*, 367, 469
- Davis, B. L., Berrier, J. C., Shields, D. W., et al. 2012, *ApJS*, 199, 33
- Elmegreen, B. G., & Elmegreen, D. M. 1990, *ApJ*, 355, 52
- Foyle, K., Rix, H.-W., Dobbs, C. L., Leroy, A. K., & Walter, F. 2011, *ApJ*, 735, 101
- Grand, R. J. J., Kawata, D., & Cropper, M. 2012, *MNRAS*, 426, 167
- Lin, C. C. and Shu, F. H. 1964, *ApJ*, 140, 646
- Marochnik, L. S. 1983, *Astrofizika*, 19, 495
- Mart nez-Garc a, E. E., Gonz alez-L pezlira, R. A., & Bruzual-A, G. 2009, *ApJ*, 694, 512
- Mart nez-Garc a, E. E., & Gonz alez-L pezlira, R. A. 2015, *Highlights of Astronomy*, 16, 323
- Merrifield, M. R., Rand, R. J., & Meidt, S. E. 2006, *MNRAS*, 366, L17
- Mishurov, Y. N., & Zenina, I. A. 1999, *A&A*, 341, 81
- Miller, R., Kenefick, D., Kenefick, J., et al. 2019, *ApJ*, 874, 177
- Patsis, P. A., Skokos, C., & Athanassoula, E. 2003, *MNRAS*, 346, 1031
- Peterken, T. G., Merrifield, M. R., Arag n-Salamanca, A., et al. 2019, *Nature Astronomy*, 3, 178
- Pour-Imani, H., Kenefick, D., Kenefick, J., et al. 2016, *ApJ*, 827, L2
- Puerari, I., & Dottori, H. 1997, *ApJ*, 476, L73
- Scarano, S., & L pine, J. R. D. 2013, *MNRAS*, 428, 625
- Seigar, M. S., Kenefick, D., Kenefick, J., & Lacy, C. H. S. 2008, *ApJ*, 678, L93
- Sellwood, J. A., & Carlberg, R. G. 2014, *ApJ*, 785, 137
- Sellwood, J. A. 2012, *ApJ*, 751(1), 44
- Sellwood, J. A., & Carlberg, R. G. 1984, *ApJ*, 282, 61
- Si-Yue Yu and Luis C. Ho. 2018, *ApJ*, 869(1), 29
- Shields, D. W., Boe, B., Pfountz, C., et al. 2015, arXiv:1511.06365
- Shu, Frank H. 2016, *Six Decades of Spiral Density-Wave Theory*, *Annual Review of Astronomy and Astrophysics*, Vol 54, Sep 2016
- Stetson, P. B. 1987, *PASP*, 99, 191
- Sundin, M. 2006, *International Journal of Astrobiology*, 5, 325
- Toomre, A. 1969, *ApJ*, 158, 899
- Tremaine, S., & Weinberg, M. D. 1984, *ApJ*, 282, L5
- Yuan, C., & Grosbøl, P. 1981, *ApJ*, 243, 432